J. Synchrotron Rad. (1998). **5**, 542–544

Twin helical undulator beamline for soft X-ray spectroscopy at SPring-8

Y. Saitoh,[a]* T. Nakatani,[a] T. Matsushita,[b] T. Miyahara,[c] M. Fujisawa,[d] K. Soda,[e] T. Muro,[f] S. Ueda,[f] H. Harada,[f] A. Sekiyama,[f] S. Imada,[f] H. Daimon[g] and S. Suga[f]

[a]JAERI-RIKEN SPring-8 Project Team, Kamigori, Ako-gun, Hyogo 678-12, Japan, [b]Japan Synchrotron Radiation Reseach Institute, Kamigori, Ako-gun, Hyogo 678-12, Japan, [c]Department of Physics, Tokyo Metropolitan University, Tokyo 192-03, Japan, [d]SRL, ISSP, The University of Tokyo, Tanashi, Tokyo 188, Japan, [e]School of Engineering, Nagoya University, Nagoya 464-01, Japan, [f]Department of Material Physics, Osaka University, Osaka 560, Japan, and [g]Graduate School of Material Science, Nara Institute of Science and Technology, Nara 630-01, Japan.
E-mail: ysaitoh@spring8.or.jp

(*Received 4 August 1997; accepted 8 December 1997*)

A very high resolution soft X-ray beamline, BL25SU, has been designed and is under construction at SPring-8. Completely right or left circularly polarized light is supplied on a common axis of a newly designed twin helical undulator. A helicity modulation up to 10 Hz can be performed using five kicker magnets. The fundamental radiation covers the region 0.5–3 keV. Higher-order radiation is rather weak on the axis. A monochromator with varied-line-spacing plane gratings is installed to cover the region below 1.5 keV. A very high resolution beyond 10^4 is expected for the whole energy region.

Keywords: soft X-ray spectroscopy; twin helical undulators; varied-line-spacing plane gratings.

1. Introduction

Integrated studies of electronic, magnetic and geometrical structures are now becoming more and more necessary. Soft X-ray spectroscopy, such as photoemission, photoelectron diffraction and magnetic circular dichroism, using circularly polarized undulator radiation is the means to satisfy such requirements. Higher-order light rejection, helicity modulation, as well as high-resolution measurements, will open up wider applications.

2. Light source and monochromator

Our light source is the 'twin helical undulator' consisting of two left- and right-handed helical undulators installed in tandem in a 4.5 m straight section. This device was designed by Kitamura's group (Hara *et al.*, 1998) and covers the energy range 0.5–3 keV with fundamental radiation. Previously developed helical undulators which produce both helicities emit light on slightly different optical axes (Goulon *et al.*, 1996). In our undulator, each helicity light comes out on the same optical axis (0 direction) and the helicity can be alternatively reversed by the five kicker magnets as shown in Fig. 1. The circularly polarized light with unwanted helicity comes out in the off-axis direction (1 direction) and can be absorbed by the water-cooled components of a mask and an *xy* slit set downstream. Quick helicity modulation up to 10 Hz or more with a switching time within 50 ms is the target.

The exclusive use of the circularly polarized light from the helical undulator of a high-energy storage ring has some characteristic advantages. First, the on-axis power density from the helical undulator is very low, especially for high K values, compared with that of the planar undulator, because most of the higher harmonics radiation is emitted off the axis of the helical undulator. Fig. 2 shows results calculated from the storage ring parameters for the power density and photon flux density (dashed and solid curves, respectively; the horizontal arrows indicate the corresponding ordinates). The dashed curves on the left-hand side of Fig. 2 have two maxima at $\theta_x = \pm\theta_m$ and a minimum at $\theta_x = 0$ corresponding to the upper geometry of Fig. 1 (Kitamura, 1996). The two different dashed curves shifted by 300 μrad correspond to the radiation from the RCP (right circularly polarized) and LCP (left circularly polarized) undulators in the upper configuration of Fig. 1. For example, the on-axis power density of each undulator at $K = 3.0$ (corresponding to the fundamental energy $\varepsilon_1 = 500$ eV) for the stored current of 100 mA is about 0.2 kW mrad^{-2} for the total radiation power of 0.8 kW and θ_m is about 190 μrad. The photon flux density for a 0.1% bandwidth at $\varepsilon_1 = 500$ eV is still as high as 2.6×10^{16} photons s^{-1} mrad^{-2} on the axis, as shown by the solid curve. Under this condition, the opposite helicity radiation along the 1 direction has the distribution shown on the right-hand side of Fig. 2.

When the helicity is changed from the upper geometry to the lower geometry in Fig. 1, undesirable radiation passes through the optical axis (0 direction) depending on the angle, θ_k, between the radiation directions of 0 and 1. θ_m decreases with decreasing K value as approximated by $K/\gamma \simeq 64K$ mrad.

The value of θ_k between the two directions (0 and 1) is so determined that the power from the unused undulator is sufficiently suppressed in using a particular helicity. Restriction of the power supply for the kickers is also taken into account. As a result, θ_k is set to 300 μrad, where the power density in the 0

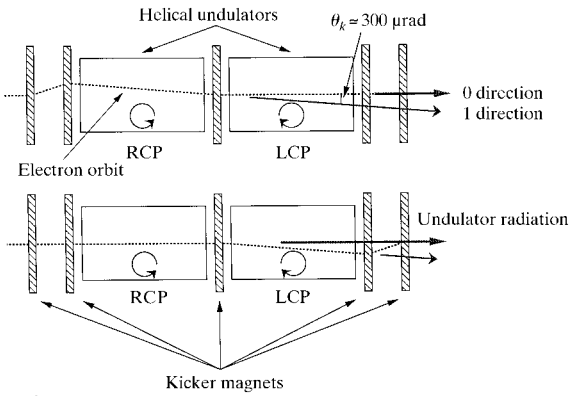

Figure 1
Schematic layout of the twin helical undulator system ($\lambda_u = 12$ cm, $N_{\rm period} = 12 \times 2$) for the left and right circularly polarized lights (represented by LCP and RCP). These undulators are installed in tandem in the straight section. Five kicker magnets switch the helicity. The thick dashed lines show the electron orbit. The 0 direction corresponds to the optical axis. The unused undulator radiation is centred along the 1 direction. The angle between the two directions is defined as θ_k.

Table 1
Parameters of optical elements of the beamline (top) and design parameters of the gratings (bottom).

Optical element	Type	Blank material (coating)	Size (W × L × T) (mm)	Radius of curvature (m)	Included angle (°)
M_h	Bendable cylindrical mirror	Si (Au)	40 × 500 × 30	>1000	177
M_v	Spherical mirror	Si (Au)	40 × 450 × 40	611	177
M_1	Spherical mirror	Si (Au)	40 × 350 × 40	418.5	177
M_2	Spherical mirror	Si (Au)	40 × 350 × 40	256	175
G	Varied-line-spacing plane grating	SiC (Au)	50 × 220 × 20	–	176 and 174
M_3	Cylindrical mirror	SiO_2 (Au)	40 × 350 × 30	258	178
M_4	Cylindrical mirror	SiO_2 (Au)	40 × 250 × 30	65	176

$h\nu_0$ is the optimized photon energy, σ_0 is the central groove spacing, and b_i (i = 1, 2, 3) are the space-variation parameters.

Grating	Deviation angle	Order	$h\nu_0$ (eV)	σ_0 (mm)	b_2 (mm^{-1})	b_3 (mm^{-2})	b_4 (mm^{-3})	Blaze angle (°)	Output photon energy (keV)
G_1	176°	+1	1000	1/1000	-9.99235×10^{-5}	9.97700×10^{-9}	-9.95405×10^{-13}	0.7	1–1.5
G_2	176°	+1	500	1/600	-9.99167×10^{-5}	9.97494×10^{-9}	-9.94988×10^{-13}	0.6	0.5–1

direction is at most 1.5 kW $mrad^{-2}$ in the ε_1 range 0.5–1.5 keV covered by the monochromator described below.

In the initial stage, the energy range 0.5–1.5 keV is covered by a grating monochromator. The *L* and *M* edges of most transition-metal and rare-earth magnetic materials are covered by this energy range.

Fig. 3 schematically shows the major optical elements of BL25SU. Detailed parameters of the components are listed in Table 1. In order to preserve the source circular polarization, a grazing-incidence monochromator is used. The beamline consists of three main parts: (i) the pre-focusing mirrors, M_h and M_v, in a hutch, (ii) the monochromator, from the entrance slit S_1 to the exit slit S_2, and (iii) the post-focusing mirrors, M_3 and M_4. A variably bendable cylindrical mirror, M_h, horizontally deflects the undulator radiation by 3° and horizontally converges the light onto the sample positions (ST_1–ST_3). The spherical mirror, M_v, vertically focuses the beam onto the entrance slit. Water-cooled Si substrates are used for these optical components to minimize possible effects of thermal instability. The water-cooled entrance slit is continuously variable from 2 μm to 1 mm.

A varied-line-spacing plane grating is mounted in this monochromator. A constant-deviation type is employed in contrast to the monochromators designed by Itou *et al.* (1989) or by Fujisawa *et al.* (1996). The type of monochromator employed here was first designed by Hettric (1988) using a spherical mirror and a varied-line-spacing plane grating. The present design has two angles of deviation, 176 and 174°, to cover the wide photon energy range from 200 to 1500 eV, by *in situ* selecting of one of the spherical mirrors, M_1 and M_2, and one of the three gratings, G_1, G_2 and G_3. For the 174° deviation angle, mirror M_1 is retracted from the beam path. One of the gratings is selected by a linear translation mechanism. The gratings are mechanically ruled in the Au thin film deposited on an SiC substrate to avoid the heat load problem. Such mechanically ruled varied-line-spacing plane gratings are used in the BL-19B planar undulator beamline at the Photon Factory and have shown high-resolution performance. However, simultaneous rotation of a large plane mirror and the grating to scan the wavelength induced some problems with the wavelength reproducibility and mechanical stability in the design by Fujisawa *et al.* (1996). In the present monochromator, the wavelength scanning only requires a rotation of the grating around an axis parallel to the grooves. Consequently, high precision of the wavelength scanning is expected. The spherical mirror, M_1 or M_2, converges the vertically divergent beam from S_1 to a virtual source at a distance 10 m from the grating centre. This type of monochromator has the excellent feature that the focal point of the grating is almost unchanged near the exit slit throughout the scanning range, when the space-variation parameters of the grating are properly determined.

The groove-spacing profile is determined from a light-path function theory. In the case of a mechanically ruled plane grating,

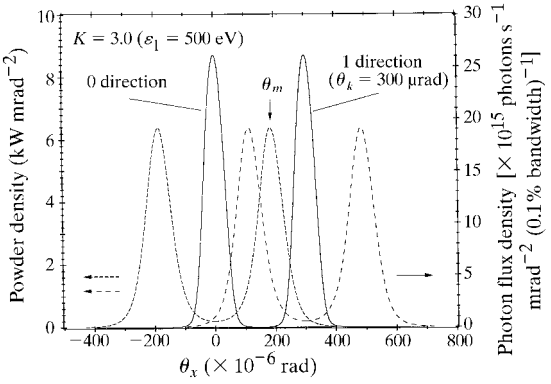

Figure 2
Horizontal distribution of the power density (dashed curves) and photon flux density (solid curves) of the radiation from the twin helical undulator. θ_k is set to 300 μrad. The power density for the 0 direction shows two peaks at angles of $\pm\theta_m$ from the central axis.

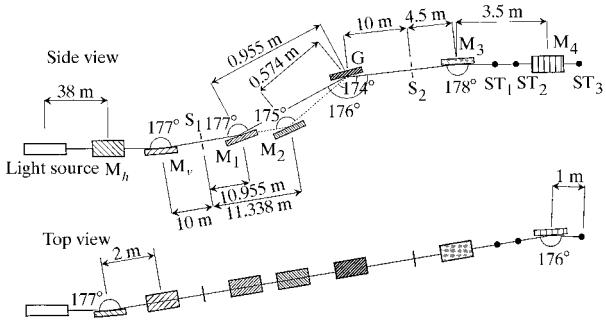

Figure 3
Schematic layout of BL25SU at SPring-8, consisting of the pre-focus mirrors (M_h and M_v), a monochromator (S_1–M_1 or M_2–G–S_2) and the post-focusing mirrors (M_3 and M_4). The monochromator is a constant-deviation type in combination with the spherical mirror (M_1 or M_2) and the varied-line-spacing plane grating. Two experimental stations (ST_1 and ST_2) are located between M_3 and M_4. A small spot size is obtained at the position of the ST_3 station.

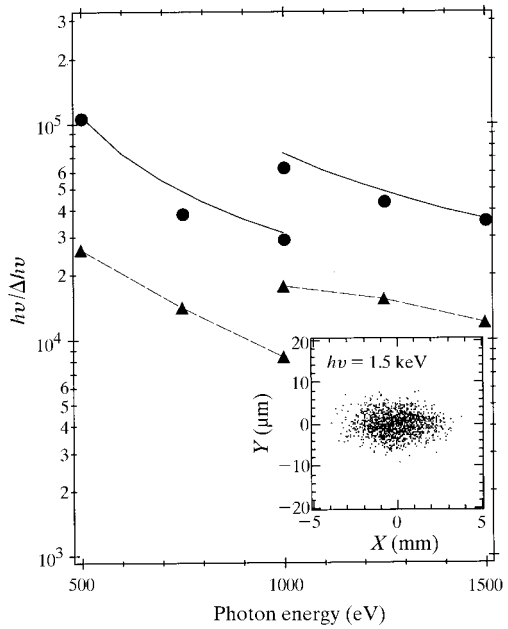

Figure 4
Estimated resolution of the monochromator by ray tracing. The entrance-slit width was set to be 10 μm. Full circles (full triangles and dashed curves) show the results for no slope error (finite slope errors of 1 μrad and 0.5 μrad for the M_1 and grating surfaces, respectively). Solid curves show entrance slit-width-limited resolution. The inset shows the image of the 10 μm entrance slit on the exit-slit plane for a photon energy of 1.5 keV for ideal optics obtained by ray tracing. The dispersion direction is along the y coordinate.

the groove spacing, σ, is given by

$$\sigma = \sigma_0/(1 + 2b_2w + 3b_3w^2 + 4b_4w^3 + \ldots),$$

where σ_0 is the central groove spacing and w is the distance along the grating length. The space-variation parameters b_2, b_3 and b_4 can be determined by cancelling the aberration terms of defocus (F_{20}), coma (F_{30}) and spherical aberrations (F_{40}), respectively, at a certain photon energy. The parameters are optimized for $h\nu_0$ in Table 1, so that high energy resolution is realized in the scanning range. Other designed parameters of the gratings G_1 and G_2 are also summarized in Table 1. The blaze angles are determined to give the highest output considering the diffraction efficiency and the reflectivity.

The designed performance of the monochromator is evaluated by ray tracing. The resolving power, $h\nu/\Delta h\nu$, of the monochromator estimated by this ray-tracing method is shown in Fig. 4. The beam characteristics were calculated from storage ring parameters (Kitamura, 1996). $\Delta h\nu$ was given by FWHM $\times$ (reciprocal linear dispersion). The width of the entrance slit is assumed to be 10 μm. The full circles are the results obtained by neglecting the slope error on the surface of the optical components and the triangles represent the results with possible slope errors (1 μrad for M_1 and 0.5 μrad for G_1). The inset of Fig. 4 shows an example of the ray tracing on the exit plane for a photon energy of 1.5 keV for the combination of M_1 and G_1, where no slope errors are assumed. Comparison of the image size with the value evaluated from magnification has shown that the contribution of aberrations is 1 μm or so. That is, it provides an almost source-size-limited resolution. The entrance slit-width-limited resolution curves are also shown for comparison by the solid curves in Fig. 4. Although the resolution strongly depends on the slope error of the optical components, we can conservatively expect a resolution of about 10^4 or more for the present system.

At ST_3 of the third experimental end-station, we expect an intensity of the order of 10^{11} photons s^{-1} at a resolving power of 10^4 with a beam size of less than 1 mm^2, considering the transmittance obtained by the ray tracing, reflectivity and grating efficiency.

3. End-stations

Three experimental stations are on this beamline. (i) High-resolution photoemission apparatus composed of an SES200 spherical mirror analyser combined with a closed-cycle liquid-He cryostat is located at ST_1 in Fig. 3. (ii) Apparatus for spectroscopy of magnetic circular dichroism of core absorption, in which the sample temperature is also controlled by a liquid-He cryostat. At present, two permanent-magnet dipoles are used for changing the direction of the magnetization. In future, a superconducting magnet will be used in combination with the rapid helicity modulation of the undulator light. (iii) A two-dimensional display-type photoelectron analyser to be used for angle-resolved photoemission and photoelectron diffraction experiments is located at ST_3 in Fig. 3. A two-dimensional photoelectron angular-distribution pattern at one particular kinetic energy is recorded simultaneously by a CCD camera. In order to realize a resolution of 1000 for the electron pass energy of the analyser, the radius of the outer hemisphere of this analyser is set to 300 mm.

The whole beamline and experimental apparatus will be commissioned in early 1998.

The authors would like to thank Professor H. Kitamura, Dr T. Hara and Dr T. Tanaka of SPring-8 for frequent and helpful discussions about the twin helical undulator. We also acknowledge many staff of the SPring-8 with whom we have discussed this beamline.

References

Fujisawa, M., Harasawa, A., Agui, A., Watanabe, M., Kakizaki, A., Shin, S., Ishii, T., Kita, T., Harada, T., Saitoh, Y. & Suga, S. (1996). *Rev. Sci. Instrum.* **67**, 345–349.
Goulon, J., Malgrange, C., Giles, C., Neumann, C., Rogalev, A., Moguiline, E., De Bergrevin, F. & Vettier, C. (1996). *J. Synchrotron Rad.* **3**, 272–281.
Hara, T., Tanaka, T., Tanabe, T., Marechal, X. M., Kumagai, K. & Kitamura, H. (1998). *J. Synchrotron Rad.* **5**, 426–427.
Hettric, M. C. (1988). *Nucl. Instrum. Methods*, A**266**, 404–413.
Itou, M., Harada, T. & Kita, T. (1989). *Appl. Opt.* **28**, 146–153.
Kitamura, H. (1996). *Insertion Device Handbook '96*, pp. 83–124. Japan Synchrotron Radiation Reseach Institute, Japan. (In Japanese.)